Taylor dispersion analysis for measurement of diffusivity and size of gadolinium-based contrast agents

Chutintorn Somnin, Laurent Leclercq, Joseph Chamieh, Mael Le Menedeu, Christelle Medina, Olivier Rousseaux, Raphaël Tripier, Carlos Platas Iglesias, Hervé Cottet

Taylor dispersion analysis for measurement of diffusivity and size of gadolinium-based contrast agents

Chutintorn Somnin[1], Laurent Leclercq[1], Joseph Chamieh[1], Mael Le Menedeu,[2,3], Christelle Medina[2], Olivier Rousseaux[2], Raphael Tripier[3], Carlos Platas Iglesias[4], Hervé Cottet[1]**

[1]IBMM, University of Montpellier, CNRS, ENSCM, Montpellier, France

[2]GUERBET Research&Innovation, BP57400, 95943 Roissy CDG Cedex, France

[3]University of Brest, UMR-CNRS 6521 CEMCA, 29238 BREST, France

[4]Facultade de Ciencias, Universidade da Coruña, 15008 - A Coruña, Spain

[*] CORRESPONDING AUTHOR

Tel: +33 4 4879 2179, E-mail: joseph.chamieh@umontpellier.fr

Tel: +33 4 6714 3427, E-mail: herve.cottet@umontpellier.fr

ABSTRACT

Gadolinium-based contrast agents (GBCA) are complexes of a Gadolinium metal center and a linear or macrocyclic polyamino-carboxylic acid chelating agent. These agents are employed to enhance the visibility of deep abnormalities through MRI techniques. Knowing the precise dimensions of various GBCA is key parameter for understanding their in-vivo and pharmaco-kinetic behaviors, their diffusivity, as well as their relaxivity. However, conventional size characterization techniques fall short when dealing with these tiny molecules (≤1 nm). In this work, we propose to determine the size and diffusivity of gadolinium-based contrast agents using Taylor dispersion analysis (TDA). TDA provided a reliable measurement of the hydrodynamic diameter and the diffusion coefficient. The obtained results were compared to DOSY NMR (Diffusion-ordered Nuclear Magnetic Resonance Spectroscopy) and DFT (Density Functional Theory).

KEYWORDS. Taylor dispersion analysis, diffusion coefficient, hydrodynamic diameter, gadolinium-based contrast agents, magnetic resonance imaging agents.

1. Introduction

Nuclear magnetic resonance imaging took off at the end of the 1980s with the appearance of the first Gadolinium-based Contrast Agents (GBCA) dedicated to this medical imaging modality (Lauffer, 1987). These agents are widely used for certain indications to improve natural contrast and enhance diagnostic accuracy, especially for the diagnosis and characterization of brain tumors. GBCA currently used in human clinical practice are small gadolinium complexes with the metal in oxidation state +III. Their action on the signal is based on the magnetic properties of Gd^{3+}, which has seven unpaired electrons distributed isotopically in the seven 4f orbitals. Gadolinium belongs to the lanthanide family and is toxic as a free ion, since it can compete with calcium in essential physiological processes (Spencer et al., 1997). To overcome this toxicity problem, Gd^{3+} must be efficiently complexed with suitable ligands while retaining its paramagnetic properties. The agent itself is not visible in MRI, but its effects on protons in its immediate neighborhood are monitored. The intensity of the signal depends not only on the local density of proton nuclei, but also on their characteristic relaxation times (Caravan, 2006). The paramagnetic relaxation effect originated by the agent makes any surrounding hydrogen atoms from water molecules to relax more efficiently, and this relaxation enhancement (also called relaxivity) generates contrast on T_1- or T_2-weighted imaging sequences. For small gadolinium complexes, the relaxivity is proportional to the number of water molecules q in the first coordination sphere, and to the rotational correlation time (τ_R) (Dumas et al., 2010). It is possible to increase τ_R by increasing the molar mass of the complex (i.e. the size of the complex). Indeed, if the rotational dynamics of the complex are approximated to a simple sphere, τ_R can be estimated from the Debye Stokes equation:

$$\tau_R = \frac{4\pi\eta r^3}{3k_B T} \quad (1)$$

where r is the radius of the sphere, η is the viscosity of the medium, k_B is Boltzmann's constant and T is the temperature. Molar mass alone does not mean that τ_R will increase in an optimal way. Local segmental flexibility can allow the Gd complex moiety to rotate rapidly while the overall motion is much slower.

The biological fate of GBCA in the body is also a crucial scientific topic. GBCAs diffuse quickly after rapid intravascular injection (bolus) distributed in the different anatomical territories. They are then eliminated mainly by the renal route in unchanged form by glomerular filtration. Their plasma half-life is of the order of 1 to 2 hours (Le Mignon et al., 1990; Staks et al., 1994; Hao et al., 2019). Nevertheless, traces of gadolinium can be detected at later times in deep or elimination organs. For example, it has been shown that some patients who have received repeated doses of GBCA show cerebral hypersignals in the dentate nucleus 1 month after injection (Kanda et al., 2016). More recently, accumulation of GBCA in the kidney, not detectable by T_1 MRI, was described (Le Fur et al., 2023). Different physicochemical parameters can play a role in the fate and elimination of GBCA in the body. The chemical stability of the GBCA, its diffusivity which is related to its hydrodynamic size, and the viscosity of the formulation can influence the diffusion of the product within the various anatomical territories (Jacquier et al., 2008)

From this introductive overview, it clearly appears that the ability to accurately measure the size (and diffusion coefficient) of GBCA can contribute to understand their *in vivo* behavior and paramagnetic efficiency. The usual techniques such as dynamic light scattering (DLS) and electron microscopy (SEM) are suitable for polymers or nanoparticles analysis (Xu, 2015) but not for molecules of low molar mass such as GBCA. In this context, Taylor dispersion analysis (TDA) seems promising as an alternative sizing technique. Indeed, TDA, which is based on the measurement of peak broadening of a solute plug in a laminar Poiseuille flow (Taylor, 1954; Aris,1956), enables the calculation of the molecular diffusion

coefficient (D) across a large range of hydrodynamic diameter (D_h, from angstrom up to 300 nm) (Belongia and Baygents, 1997; Chamieh et al., 2017). TDA is performed using narrow bore fused silica capillaries (typically ~50 µm i.d.). It presents several advantages such as low sample consumption (few nL are injected for each analysis), no sample filtration (insensitive to the presence of dusts), absolute method (no size calibration), rapid analysis time and automation.

In this work, the diffusivity and the hydrodynamic radius of various commercial or under-development gadolinium complexes were measured by TDA and compared to diffusion-ordered NMR spectroscopy (DOSY) and Density Functional Theory (DFT) calculations.

2. Materials and methods

2.1 Materials

Structurally, there are 2 distinct categories of GBCA: 1. Macrocyclic molecules in which the Gd^{3+} ion is caged within the cavity of the ligand, and 2. Open-chain or "linear" molecules (Table S1). Within each category, there are both ionic and neutral GBCA. Gd-DTPA-BMA (Gadodiamide, Omniscan® GE-Healthcare) and Gd-BOPTA (Gadobenate dimeglumine, MultiHance® Bracco) were diluted to 5 mM in ultrapure water coming from a Milli-Q system from Millipore (Molsheim, France). Gd-DOTA (Gadoterate meglumine, Dotarem® Guerbet), Gd-HP-DO3A (Gadoteridol, ProHance® Bracco), Gd-BT-DO3A (Gadobutrol, Gadovist® Bayer Healthcare), Pyclen based structure derivatives (PCTA) were diluted to 5 mM using 10 mM Tris-HCl buffer pH 7.4 (tris(hydroxymethyl)aminomethane, Sigma-Aldrich, France).

PCTA derivatives were prepared using previously reported protocols for D1 and D2 (Gadopiclenol, Elucirem® Guerbet) (Port et al., 2008) and for D3 (Port et al., 2000). The

Europium or Yttrium analogue complexes were prepared using respectively europium or yttrium chloride at the complexation step.

The fluorescence emission spectra were measured using a fluorescence spectrofluorometer (Jasco, FP-8300, UK).

2.2 Taylor dispersion analysis

All experiments were performed on an Agilent 7100 CE system (Waldbronn, Germany) equipped with a diode array UV-visible detector and with a Zetalif LED-induced fluorescence detector (λ_{ex} 275 nm) purchased from Adelis (Toulouse, France). Analyses were conducted in a bare fused-silica capillary (Polymicro technologies, USA) having a 50 µm i.d. with a total length of 65 cm. The position of the LEDIF and UV detection windows were at 44 and 56.5 cm from the inlet side, respectively, which allows for simultaneous detection from both detectors (Fig. 1).

Before analysis, capillaries were conditioned by flushing (at 1 bar) with water for 20 min followed by the background electrolyte (BGE) for 20 min. A 10 mM Tris buffer at pH 7.5 was used as BGE for all samples except for Gd-DTPA-BMA and Gd-BOPTA, where water was used. Samples were prepared in the BGE and injected continuously at 100 mbar from the inlet side of the capillary. Between each run, the capillary was rinsed by flushing with the BGE for 5 min. UV detection was performed at 200 nm with a bandwidth of 4 nm. The fluorescent signals were measured at an excitation wavelength of 275 nm and the signals were collected from 300 to 450 nm or from 300 to 330 nm depending on the collection signal filter. Analyses were performed at 25°C and the sample carrousel was also kept at 25°C using an external circulating water bath (Instrumat, France). Signal was acquired using Chemstation software, then exported to Microsoft excel for subsequent data treatment.

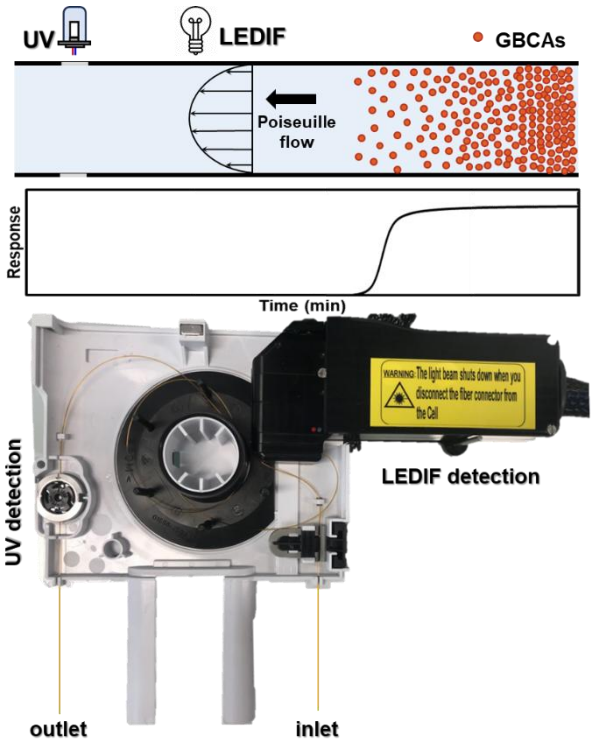

Fig. 1. Scheme of an Agilent capillary electrophoresis cassette showing the positions of the LEDIF and UV detectors used for GBCA Taylor dispersion analysis. The upper part represents the frontal mode analysis in TDA.

2.3 Data treatment

The temporal variance σ^2 of the dispersion profile from the TDA experiment in frontal mode was obtained by fitting the elution front with a Gaussian error function (*erf*) (d'Orlyé et al., 2008; Taylor, 1953) using equation (2):

$$y = \frac{1}{2} + \frac{1}{2} erf \frac{(t - t_0)}{\sigma\sqrt{2}} \quad (2)$$

The sample's diffusion coefficient D and hydrodynamic radius D_h were obtained from equation (3) and equation (4) respectively.

$$D = \frac{R_c^2 t_0}{24\sigma^2} \quad (3)$$

$$D_h = \frac{k_B T}{3\pi\eta D} \quad (4)$$

where R_c is the capillary radius (m), t_0 is the average elution time (s), T is the temperature (K) and η is the viscosity of the carrier liquid (Pa s). The two conditions of validity of TDA

expressed by τ and *Pe* numbers and calculated using inequations (5) and (6) (Taylor, 1954; Chamieh and Cottet, 2014; Cottet et al., 2014) were fulfilled:

$$\tau = \frac{D t_0}{R_c^2} \geq 1.25 \quad (5)$$

$$Pe = \frac{u R_c}{D} \geq 40 \quad (6)$$

where τ is an dimensionless characteristic time, *Pe* is the Peclet number and u is the linear mobile phase velocity (m s^{-1}). Inequation (5) is verified when the characteristic diffusion time of the solute in the capillary cross section is much lower than t_0 . Inequation (6) is valid when the axial diffusion of the solute is negligible compared to Taylor dispersion.

In order to measure the viscosity of the carrier liquid, the capillary was filled with BGE. Then, a 0.1% (v:v) DMF solution in BGE was continuously injected at 100 mbar. The DMF was detected at 200 nm. The mean elution time of DMF (t_{DMF}) was measured, and the relative viscosity (η) was calculated by comparing it to the elution time with pure water (t_0) at the same temperature. The viscosity, being proportional to the elution time, is given by equation (7) with about 3% precision (Bello et al., 1994):

$$\eta = \frac{t_{DMF}}{t_0} \eta_0 \quad (7)$$

where η_0 is the viscosity of water at the same temperature. In this work, the viscosity of tris buffer was found to be similar to the viscosity of water (8.92×10^{-4} Pa s).

2.4 Diffusion Ordered Spectroscopy (DOSY)

The method is based on a pulsed field gradient (PFG) and a stimulated spin echo (STE) experiment. Analysis of the exponential decay of the signal obtained with different pulse frequencies gives the diffusion coefficient *D*. This method can therefore be used to assess the size with the Stokes-Einstein equation (equation (4)), which applies in the case of a solute

assumed to a hard sphere, with a hydrodynamic diameter D_h and evolving in a continuous medium.

DOSY NMR spectra were recorded at 25°C on a BRUKER AVANCE III HD 500 spectrometer equipped with an indirect 5 mm probe head BBFO 1H/{BB}. NMR analyses were performed on samples obtained by dissolution of 10 mg of product in 700 µL of D_2O. The spectra were performed according BRUKER's pulse programs with standard pulse sequences of 1.5 s of delay, a 30° pulse and 16 scans. Viscosity of D_2O (298K): 1.1×10^{-3} Pa s (Evans et al., 2013). Data processing was carried out using MestReNova software (Mestrelab Research) Version 14.1.0-24037.

2.5 Density Functional Theory (DFT)

All calculations were performed with the Gaussian 16 program package (Frisch et al., 2016), within the frame of density functional theory (DFT). We selected the hybrid, long-range corrected, wB97XD density functional, which includes atom–atom dispersion corrections (Chai and Head-Gordon, 2008). We have shown recently that this functional provides good results for Gd complexes in terms of bond distances of the metal coordination environment and relative stability of different coordination numbers (Nucera et al., 2023). In these calculations we employed a small-core effective core potential for gadolinium (28 electrons in the core) (Dolg et al., 1989) and the associated ECP28MWB_GUESS basis set. The Def2-TZVPP basis set was employed for all other atoms (Weigend and Ahlrichs, 2005). All Gd complexes were modelled using the unrestricted method in their high-spin configuration (octet). For Y complexes we used a restricted calculations with the ECP28MDF (28 electrons in the core) and its associated VTZ basis set (Peterson et al., 2007). The integration grid was set with the integral: superfine grid keyword. Bulk water solvent effects were incorporated using a polarizable continuum model with the default options implemented in Gaussian (IEFPCM) (Tomasi et al., 2005). Molecular volumes were estimated using the

196 volume = tight keyword. Input geometries for geometry optimization were obtained from
197 previous computational works (Regueiro-Figueroa and Platas-Iglesias, 2015; Esteban-Gómez
198 et al., 2012). Frequency calculations were performed to ensure that the optimized geometries
199 correspond to local energy minima.

200 ## 3. Results and discussion

201 This work aims to determine the diffusivity and the hydrodynamic diameter of various
202 GBCA with different molar masses ranging from 500-3500 g mol^{-1} by TDA and to compare
203 the results with DOSY-NMR and DFT calculations. For a matter of comparison with DOSY-
204 NMR, which cannot be done on GBCA directly due to their paramagnetic properties, yttrium
205 analogues were synthetized and studied by both TDA and DOSY-NMR. To evaluate the
206 fluorescence response in TDA, the europium derivatives were also synthesized and
207 investigated in comparison with GBCA. Since the UV and the fluorescence responses can be
208 very different depending on the chemical structure of GBCA, the limits of detection were
209 first determined for both detection modes, as discussed in the following section.

210 ### 3.1 UV and Emission spectra of Gadolinium complexes

211 The UV and fluorescence responses of the different GBCA were investigated at the
212 same concentration of 5.0 mM. Fig. 2A shows the UV-visible spectra of the different
213 samples. As can be seen Gd-HP-DO3A, Gd-BT-DO3A and Gd-DOTA had low UV response
214 and could only be analyzed at a wavelength lower than 200 nm, where the absorption of the
215 carboxyl groups takes place (Xu et al., 2002). However, Gd-PCTA D1, Gd-PCTA D2 and
216 Gd-PCTA presented an absorption maximum at 270 nm, characteristic of the pyridyl
217 chromophore (Pellegatti et al., 2008), while Gd-PCTA D3 showed a maximum at 230 nm due
218 to aromatic cycle on each of the three pendant arms. As for Gd-DTPA-BMA and Gd-
219 BOPTA, the UV response was maximum and intense at 200 nm. For the subsequent TDA

220 analysis of the different GBCA, a common wavelength of 200 nm was used to size the
221 different samples.

222 In Fig. 2B, the emission spectra of GBCA are presented at an excitation wavelength of
223 275 nm. The results show that Gd-HP-DO3A, Gd-DOTA, Gd-BT-DO3A and Gd-DTPA-
224 BMA had a sharp emission peak at 315 nm in their decreasing order of emission intensity.
225 This emission band is characteristic of the $^{6}P_{7/2} \rightarrow {}^{8}S_{7/2}$ transition of Gd(III), which is
226 quenched by the presence of aromatic chromophores (Bünzli, 2010). GBCA samples
227 containing aromatic units (Gd-PCTA, Gd-PCTA D1 and Gd-PCTA D2) exhibited low
228 fluorescence emission at 300 nm, as shown in Fig. S2. Conversely, Gd-BOPTA and Gd-
229 PCTA D3 showed a non-significant fluorescence response leading to a nonlinear response in
230 the studied concentration range. Therefore, for the LEDIF responding samples, a collection
231 filter of the emitted fluorescence with a collecting range between 300 - 450 nm or between
232 300 - 330 nm were used for TDA analysis.

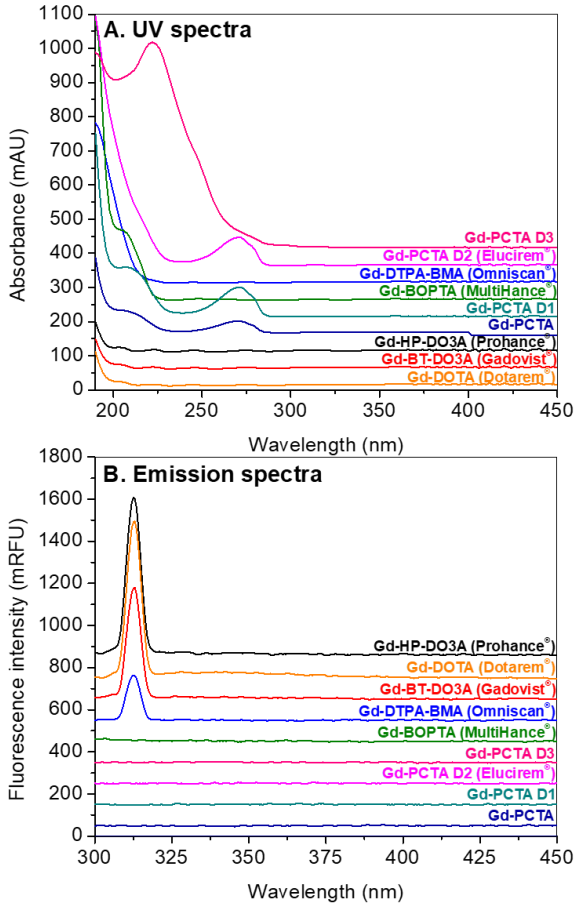

Fig. 2. (A) UV-Visible spectra and (B) emission spectra (excitation wavelength 275 nm) of Gadolinium complexes at a concentration of 5.0 mM. GBCA were diluted in 10 mM Tris-HCl buffer pH 7.4 except for Gd-DTPA-BMA and Gd-BOPTA diluted in ultrapure water. Sensitivity of spectrofluorometer was set at very low level. The emission spectra of Gd-PCTA, Gd-PCTA D1 and Gd-PCTA D2 at medium sensitivity level of spectrofluorometer are shown in Fig. S2.

3.2 Taylor dispersion analysis in frontal mode

Classically TDA is performed in plug mode, *i.e.* by injecting a small volume of the sample (less than 1% of the capillary volume to the detection point), and then the sample is mobilized with the BGE as a mobile phase. However, because of the dilution of the injection plug during the mobilization, and to enhance the sensitivity of detection, TDA in frontal mode was applied. Fig. 3 shows the elution profile of Gd-PCTA D2 with varying concentrations ranging from 0.05 to 5.0 mM by UV and LEDIF detections. The experimental elution profile was fitted using a Gaussian error function (*erf*) to obtain the variance and, consequently, to determine the molecular diffusion coefficient (D) and the hydrodynamic diameter (D_h). The fit is presented as a red dotted line in Fig. 3. The first derivative of the

elution profiles are also presented (see insert in Fig. 3), as they allow for a better visualization of the symmetry of the signal. All experimental taylorgrams of the other GBCA are presented in Fig. S3 to S10.

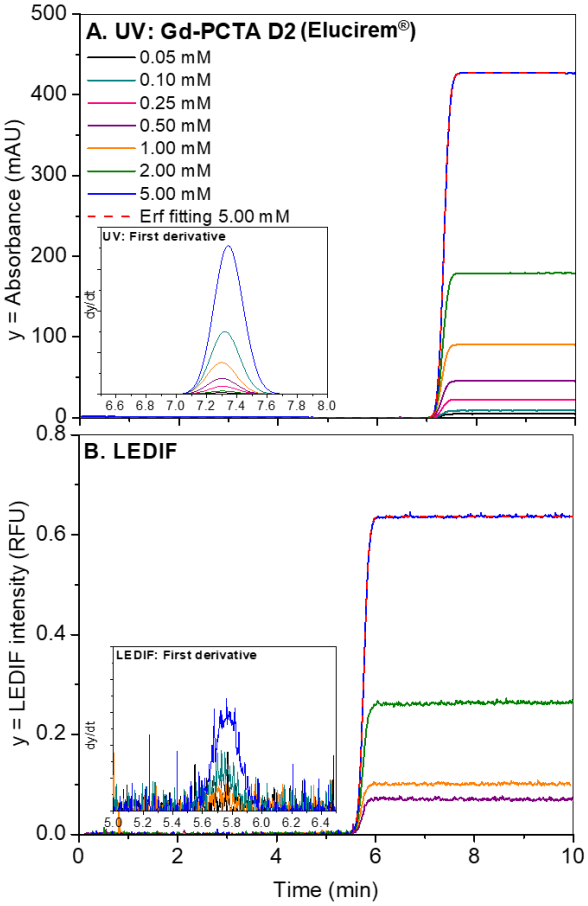

Fig. 3. Frontal taylorgrams of Gd-PCTA D2 at different concentrations using (A) UV and (B) LEDIF (λ_{ex} 275 nm, $\lambda_{collection}$ 300-450 nm) detections. *Erf* fitting to calculate D_h and D are plotted as a red dotted line. The insert represents the first derivative of the frontal taylorgrams. Experimental conditions: fused silica capillary of 65 cm total length (44 cm to LEDIF detector, 56.5 cm to UV detector) x 50 µm i.d., eluent: 10 mM Tris-HCl buffer (pH 7.4), mobilization pressure 100 mbar.

An additional advantage of the frontal mode is that the front height is directly correlated to the injected concentration. Therefore, calibration curves of GBCA were plotted and the correspondig sensitivity of detection (slope of calibration curve, *a*), the LOD and LOQ were determined and reported in Table 1 for both UV (at 200 and 270 nm) and LEDIF (λ_{ex} 275 nm, $\lambda_{collection}$ 300 - 450 nm and 300 - 330 nm) detections. GBCA with aromatic ring has relatively low LOD in UV (in the range of 0.01 – 0.26 mM). Comparatively, non-aromatic GBCA have higher LOD between 0.22 – 0.84 mM. LOD with LEDIF detection is in

interval 0.29 -1.50 mM. These results showed that the LOD of UV detection are lower than the one obtained by LEDIF detection for all GBCA, except for Gd-HP-DO3A.

D_h, and D of GBCA were determined using eq. (3) and eq. (4) applying both detection methods. Repeatabilities of TDA analysis were evaluated for each detection mode using RSD (n=6). It was found that UV detection RSD was approximately 0.2 – 1.6%, and around 0.6 – 9.4% for LEDIF detection, indicating better repeatabilities when using the UV detection, probably due to better sensivity. The relative differences in the calculated D_h between the two detection modes was very low (average difference of about 4%) except for Gd-DOTA (12%) due to the presence of meglumine, which is a counterion of the complex. Meglumine contributed to the UV response (slope at 200 nm of 1.56 AU M^{-1}) and can affect the average size with this detection mode, but not with the LEDIF detector. In the case of Gd-DOTA, the meglumine response at 200 nm corresponds to 59% of the overall signal (1:1 GBCA:meglumine molar ratio). Despite this huge contribution of the counterion to the UV signal, the impact of meglumine on the Gd-DOTA size is limited since meglumine has a comparable size as the GBCA. The LEDIF detector should be however preferred for TDA of Gd-DOTA. As for Gd-BOPTA, the response of the meglumine is about 5% of the total signal at 200 nm (1:2 GBCA : meglumine molar ratio) and therefore the impact of meglumine on the size of Gd-BOPTA is minor. It is worth nothing that for all the other contrast agents, there is no counter ions that can impact the measurement since they are neutral.

Fig. 4 gathers the calculated D_h and the corresponding diffusion coefficient D of all GBCA based on the analysis with UV at 200 nm. The results show that the D_h were in the increasing order of Gd-HP-DO3A 0.93 nm < Gd-BOPTA 0.97 nm = Gd-DTPA-BMA 0.97 nm < Gd-PCTA 0.98 nm < Gd-BT-DO3A 0.99 nm < Gd-DOTA 1.02 nm with RSD on 6 repetitions of about 1% or less. As for Gd-PCTA D1, Gd-PCTA D2 and Gd-PCTA D3, they presented larger hydrodynamic diameters of 1.16, 1.39 and 2.20 nm, respectively. It is

290 important to remind that the diffusivity (D) of the GBCA are inversely proportional to the
291 hydrodynamic diameter (D_h) and therefore do not vary linearly one each other. Diffusion
292 coefficients of about 4.7-5.0$\times 10^{-10}$ m^2s^{-1} were determined for DTPA or macrocyclic cyclen
293 based GBCA, and of about 2.2-4.2 $\times 10^{-10}$ m^2s^{-1} for Pyclen based GBCA. For PCTA
294 derivatives, there is a good proportionality between the molecular weight and the
295 hydrodynamic diameter.

Table 1. Sensitivity, LOD, LOQ, D_h and D obtained by TDA using UV and LEDIF detections

Sample	M (g mol^{-1})	aromatic	BGE	UV detection at 200 nm and 270 nm					LEDIF λ_{ex} 275 nm $\lambda_{collection}$ 300-450 nm and $\lambda_{collection}$ 300-330 nm				
				Slope (AU M^{-1})	LOD[e] (mM)	LOQ[e] (mM)	D_h (RSD) (nm)	D (10^{-10} m^{2}s^{-1})	Slope (RFU mM^{-1})	LOD[e] (mM)	LOQ[e] (mM)	D_h (RSD) (nm)	D (10^{-10} m^{2}s^{-1})
Gd-DTPA-BMA (Omniscan®)	573.6	no	Water	57.7[a]	0.10[a]	0.32[a]	0.97 (0.8%)[a]	5.00[a]	0.058[c]	0.71[c]	2.36[c]	0.97 (9.4%)[c]	5.01[c]
				n.d.[b]	n.d.[b]	n.d.[b]	n.d.[b]	n.d.[b]	0.033[d]	1.72[d]	5.72[d]	0.97 (4.9%)[d]	5.00[d]
Gd-BOPTA (MultiHance®)	653.7	yes	Water	51.2[a]	0.18[a]	0.61[a]	0.97 (0.6%)[a, f]	4.98[a, f]	n.d.[c]	n.d.[c]	n.d.[c]	n.d.[c]	n.d.[c]
				n.d.[b]	n.d.[b]	n.d.[b]	n.d.[b]	n.d.[b]	n.d.[d]	n.d.[d]	n.d.[d]	n.d.[d]	n.d.[d]
Gd-HP-DO3A (Prohance®)	558.7	no	Tris-HCl	1.96[a]	0.84[a]	2.81[a]	0.93 (1.2%)[a]	5.27[a]	0.171[c]	0.29[c]	0.97[c]	0.89 (1.3%)[c]	5.46[c]
				n.d.[b]	n.d.[b]	n.d.[b]	n.d.[b]	n.d.[b]	0.075[d]	0.76[d]	2.52[d]	0.99 (2.1%)[d]	4.89[d]
Gd-BT-DO3A (Gadovist®)	604.72	no	Tris-HCl	2.65[a]	0.70[a]	2.35[a]	0.99 (1.2%)[a]	4.86[a]	0.102[c]	1.50[c]	5.00[c]	0.95 (0.4%)[c]	5.03[c]
				n.d.[b]	n.d.[b]	n.d.[b]	n.d.[b]	n.d.[b]	0.053[d]	0.39[d]	1.28[d]	1.01 (1.0%)[d]	4.80[d]
Gd-DOTA (Dotarem®)	558.7	no	Tris-HCl	2.63[a]	0.22[a]	0.72[a]	1.02 (0.7%)[a, f]	4.79[a, f]	0.202[c]	0.56[c]	1.87[c]	0.90 (0.6%)[c]	5.46[c]
				n.d.[b]	n.d.[b]	n.d.[b]	n.d.[b]	n.d.[b]	0.094[d]	1.06[d]	3.52[d]	0.98 (1.2%)[d]	4.98[d]
Gd-PCTA	534.6	yes	Tris-HCl	26.2[a]	0.45[a]	1.50[a]	0.98 (0.5%)[a]	4.98[a]	0.150[c]	0.86[c]	2.88[c]	1.05 (4.1%)[c]	4.67[c]
				15.2[b]	0.15[b]	0.49[b]	0.97 (1.2%)[b]	5.02[b]	0.111[d]	0.52[d]	1.74[d]	1.13 (3.7%)[d]	4.33[d]
Gd-PCTA D1	750.6	yes	Tris-HCl	34.5[a]	0.26[a]	0.86[a]	1.16 (0.9%)[a]	4.22[a]	0.118[c]	0.35[c]	1.16[c]	1.16 (0.7%) [c]	4.21[c]
				17.7[b]	0.22[b]	0.75[b]	1.11 (0.2 %)[b]	4.43[b]	0.055[d]	0.50[d]	1.67[d]	1.19 (0.9%)[d]	4.08[d]
Gd-PCTA D2 (Elucirem®)	970.1	yes	Tris-HCl	85.6[a]	0.12[a]	0.40[a]	1.39 (0.4%)[a]	3.47[a]	0.129[c]	0.43[c]	1.38[c]	1.47 (0.8%)[c]	3.32[c]
				16.3[b]	0.06[b]	0.20[b]	1.43 (0.3%)[b]	3.43[b]	0.063[d]	0.88[d]	2.94[d]	1.47 (0.8%)[d]	3.33[d]
Gd-PCTA D3	3545	yes	Tris-HCl	1355[a]	0.01[a]	0.038[a]	2.20 (0.2%)[a]	2.23[a]	n.d.[c]	n.d.[c]	n.d.[c]	n.d.[c]	n.d.[c]
				141[b]	0.001[b]	0.004[b]	2.34 (1.6%)[b]	2.09[b]	n.d.[d]	n.d.[d]	n.d.[d]	n.d.[d]	n.d.[d]

[a] UV at 200 nm, [b] UV at 270 nm, [c] LEDIF using $\lambda_{collection}$ 300-450 nm, [d] LEDIF using $\lambda_{collection}$ 300-330 nm. [e] LOD, LOQ were calculated by $3\times s_{y/x}/a$ and $10\times s_{y/x}/a$, respectively, where $s_{y/x}$ is the regression standard deviation and a is the slope of the calibration curve. [f] value affected by the presence of meglumine (counterion).

Calculated D_h from 50 µm capillary (d_c was optically measured) using viscosity η = 8.92×10^{-4} Pa s at 25°C. GBCA concentration at 5.0 mM. Gd-DTPA-BMA and Gd-BOPTA diluted in ultrapure water. The other GBCA diluted in 10 mM Tris-HCl buffer pH 7.4.

n.d. = not detected

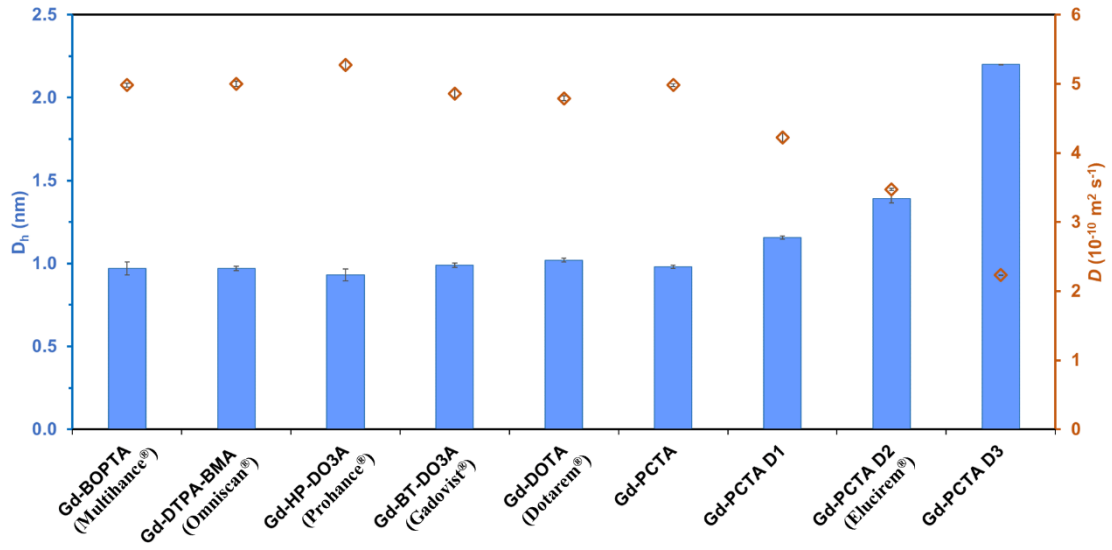

Fig. 4. Hydrodynamic diameter D_h (bar graph) and diffusivity D (diamond shape) of GBCA by TDA using UV detection at 200 nm. Experimental condition as in Fig. 3 and Table 1 (η = 8.92×10^{-4} Pa s at 25°C).

3.3 Diffusion Ordered Spectroscopy (DOSY)

Gadolinium complexes (Gd III) are highly paramagnetic due to the presence of 7 electrons on the 4f level ([Xe] 4f7). These magnetic properties interfere with NMR spectroscopy experiments. In order to overcome this difficulty, the study of isosteric complexes was proposed (Le Fur et al., 2020). The use of diamagnetic yttrium (Y(III)) complexes is one way of obtaining spectral information since these compounds have a high degree of structural similarity to Gd(III) complexes. Five yttrium complexes were prepared and DOSY experiments were carried out to evaluate their diffusion coefficients. Under our experimental conditions, the two reference complexes Y-DOTA and Y-PCTA exhibit the same D value (3.6×10^{-10} m^2 s). Similarly, for the Y-PCTA-D1 complex the measured experimental value is D = 2.9×10^{-10} m^2 s whereas the Y-PCTA-D2 complex shows a value of 2.3×10^{-10} m^2 s. These values cannot be compared directly to D values obtained by TDA due to the difference in viscosity of the medium (D_2O *vs* H_2O).

However, by applying the Stokes-Einstein relationship (viscosity of D_2O at 298K of 1.1×10^{-3} Pa s (Evans et al., 2013)), the hydrodynamic diameter of the different molecules was evaluated and compared to the ones obtained by Taylor diffusion (see Table 2). Good

correlation between the different experimental techniques was found, confirming that yttrium can be useful when the use of gadolinium is not possible.

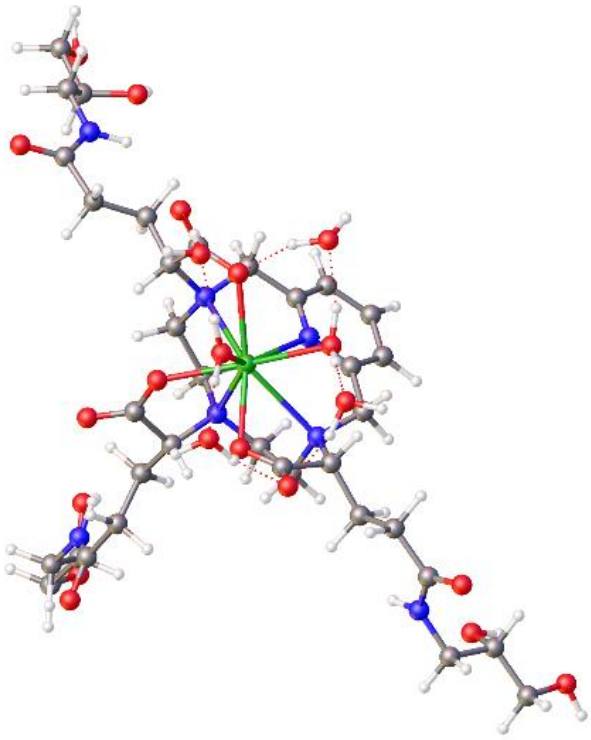

Fig. 5. Molecular structure of the Gd-PCTA D2 obtained with DFT calculations.

3.4 Density Functional Theory (DFT)

The TDA sizes of the GBCA displayed in Fig. 4 were also obtained using DFT calculations. For this purpose, the geometries of the different complexes were optimized using well-established methods (details in the computational section 2.5). It is worth mentioning that our models incorporated a few explicit second-sphere water molecules involved in hydrogen bonding with coordinated water molecules, as we demonstrated previously that this was important to describe the Gd-O_{water} distances (Esteban-Gómez et al., 2012). The representative structure of the Gd-PCTA D2 complex is shown in Fig. 5. The molecular volumes were subsequently estimated as the density envelope defined by an 0.001 e $bohr^{-3}$ isodensity surface, as recommended by Bader (Bader et al., 1987). The diameter of the complex was then estimated from the molecular volume as the diameter on a sphere with

that volume. These calculations give D_h values close to 1 nm for all small complexes: Gd-HP-DO3A (1.02 nm), Gd-BOPTA (1.08 nm), Gd-DTPA-BMA (1.04 nm), Gd-BT-DO3A (1.01 nm), Gd-DOTA (1.01 nm) and Gd-PCTA (0.98 nm). These values are in very good agreement with the experimental data, with deviations < 10%, which confirms that these small complexes are not aggregating under the conditions of formulation (also used for TDA studies). It is clear from Table 2 that, as expected, similar D_h and D values were obtained for all lanthanides (Gd, Eu and Y) with the same ligand. The corresponding diffusion coefficients estimated from the Stokes-Einstein are also in good agreement with the experimental values, as would be expected. We note that some deviations are expected from the experimental (TDA) and theoretical data (DFT). In particular, the different charge and electrostatic properties of the complexes is expected to affect the size of the second hydration shell, and thus their hydrodynamic size provided by TDA and DOSY measurements. However, the sizes obtained with DFT are estimated from the electron density.

Table 2. Comparing D_h and D by DOSY, DFT and TDA

		PCTA		PCTA D1			PCTA D2		
		Gd	**Y**	**Gd**	**Eu**	**Y**	**Gd**	**Eu**	**Y**
DOSY in D_2O	D_h (nm)[a]	NT	1.1	NT	NT	1.4	NT	NT	1.7
	D at 298K (10^{-10} m^2 s^{-1})	NT	3.6	NT	NT	2.9	NT	NT	2.3
DFT	D_h (nm)	1.03	1.03	1.17	NT	1.14	1.29	NT	1.27
	D at 298K (10^{-10} m^2 s^{-1})	4.74	4.73	4.19	NT	4.28	3.78	NT	3.85
TDA in Tris-HCl	D_h (nm)[b]	0.98 ± 0.01	1.05 ± 0.05	1.16 ± 0.01	1.29 ± 0.01	1.32 ± 0.07	1.39 ± 0.03	1.39 ± 0.04	1.46 ± 0.02
	D at 298K (10^{-10} m^2 s^{-1})	4.98 ± 0.02	4.76 ± 0.12	4.22 ± 0.07	3.80 ± 0.02	3.71 ± 0.20	3.47 ± 0.01	3.50 ± 0.12	3.36 ± 0.03

NT: Not tested

D_h : hydrodynamic diameter ; D : diffusion coefficient. All samples are 5 mM in Tris-HCl buffer for TDA.

[a] Viscosity of D_2O (298K): 1.1232×10^{-3} Pa s [b] Viscosity of Tris-HCl buffer (298K): 8.92×10^{-4} Pa s, d_c was optically measured.

Table 2 shows a comparison of calculated D_h and D between TDA and the other methods (DOSY and DFT). The NMR DOSY method cannot measure the diffusivity directly on gadolinium complexes due to their paramagnetic properties, which prevent observation of ^{1}H signals of the ligand nuclei. Conversely, TDA works for all the complexes whatever the ligand and the metal (Gd, Eu and Y). The size obtained by TDA showed a good agreement with DOSY on the yttrium diamagnetic analogues (Y-PCTA and Y-PCTA D1). The deviations in diffusion coefficient resulted from the different viscosities used in the calculation since NMR was conducted in deuterated water (more viscous than water). The diameters of Y-PCTA, Gd-PCTA D1 and Gd-PCTA D2 estimated by DFT calculations are as well comparable to the diameters determined by TDA, differing by less than 2% for Y-PCTA and Gd-PCTA D1, and by 7% for Gd-PCTA D2. We note that TDA and DOSY provide D_h data with a significant deviation. This is likely related to the different concentrations of GBCA used (5 mM for TDA, 15 mM for DOSY). In case some concentration-dependent aggregation occurs, this should have a more important effect in the size measurement performed with DOSY.

3.5 Precision of TDA measurement

According to equation (3), the diffusion coefficient is directly proportional to the square of the capillary diameter (d_c^2). Therefore, imprecision on the knowledge of the capillary diameter might cause significant errors in D and D_h calculations and may decrease the inter-capillary batch-to-batch intermediate precision of the determination. In this study, we compared D_h of 5.0 mM Gd-PCTA D2 measured on 5 different capillaries for which d_c was evaluated by 3 different approaches. The first approach consisted in using the nominal d_c (50 µm) given by the manufacturer. The second approach used the average capillary diameter values given by the manufacturer for the beginning and the end of the capillary roll (namely, 47.1 µm for capillary 1 and capillary 2, and 50.3 µm for capillaries 3, 4 and 5). The third

method was based on the experimental determination of the capillary diameter using a high-resolution optical setup in our laboratory. Fig. 6 shows the GBCA D_h allowing to estimate the inter-capillary batch-to-batch intermediate precision obtained by TDA for the 5 capillaries and the 3 different approaches for d_c evaluation. The results demonstrated that using the precise diameter of capillary by optical camera provided the best inter-capillary intermediate precision for TDA sizing (RSD = 3.6%, n=5 capillaries). However, relatively small differences in D_h between the capillaries are remaining probably due to some temperature variations during the experiment that can affect the viscosity and thus the diffusivity.

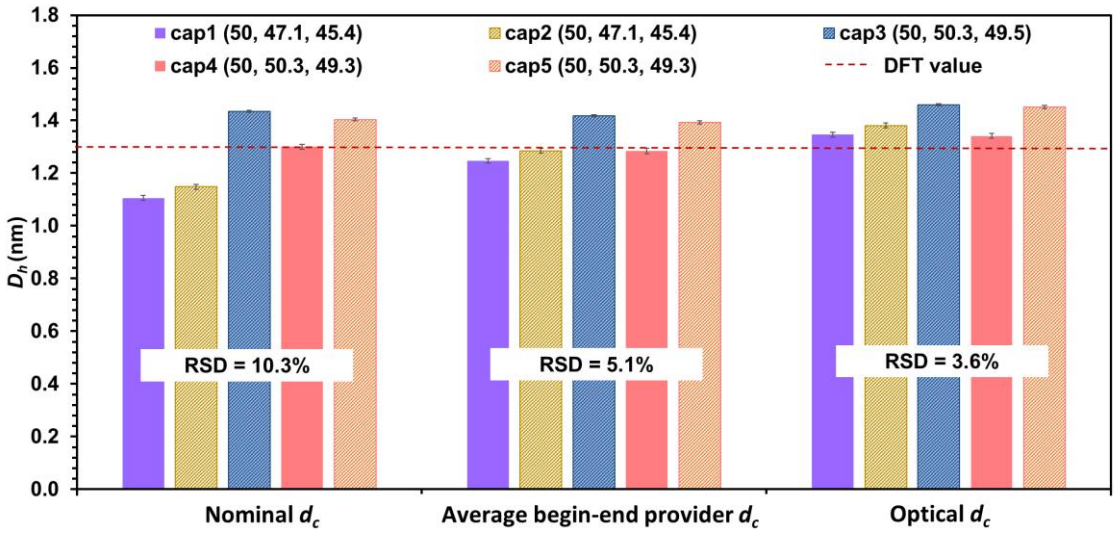

Fig. 6: Inter-capillary intermediate precision of TDA using 5 different capillaries as indicated on the graph (nominal d_c, average d_c between the begin and end values given by the capillary provider, optical d_c determined in our laboratory, all in µm) for sizing 5.0 mM Gd-PCTA D2. D_h in nm is provided using eq.(4) and the corresponding d_c value. RSD were determined based on the 5 capillaries. Errors bars on D_h were determined for each capillary based on n=6 repetitions. Experimental conditions as in Fig. 3.

4. Conclusion

The aim of this work was to determine the diffusivity and the hydrodynamic diameter of GBCA by TDA and to compare these experimental values with DOSY NMR and DFT calculations. TDA was performed using both UV and LEDIF detections, using frontal mode (continuous injection of the GBCA sample into the capillary) to increase the sensitivity of detection. This study demonstrates that both detectors provide similar D and D_h values.

However, UV detection shows a better sensitivity and lower LOD than fluorescence detection. The hydrodynamic diameters were in the order of Gd-HP-DO3A 0.93 nm < Gd-BOPTA 0.97 nm = Gd-DTPA-BMA 0.97 nm < Gd-PCTA 0.98 nm < Gd-BT-DO3A 0.99 nm < Gd-DOTA 1.02 nm < Gd-PCTA D1 1.16 nm < Gd-PCTA D2 1.39 nm < Gd-PCTA D3 2.20 nm. The TDA approach confirms that all the tested GBCA have high diffusivity in the order of 4.7-5.0× 10^{-10} m^2s^{-1}, as confirmed by an orthogonal analytic approach such as DOSY. These complexes do not aggregate in solution under the conditions used for TDA experiments, as demonstrated by sizes estimated with DFT calculations. The TDA has several advantages over NMR DOSY, as it can be directly applied to gadolinium complexes.

The pharmacokinetics and biodistribution of GBCA depends on several parameters, size being among one of them. However, other properties such as stability, polarity or electrical charge also play a critical role (Aime et al., 2009; He et al., 2024). Small extracellular are generally eliminated via the kidney by passive glomerular filtration (He et al., 2024). The largest derivative investigated here, Gd-PCTA D3, displays a different pharmacokinetic profile, as it remains in the vascular compartment for a rather long time in animal models (Jacquier et al., 2008). Furthermore, it is well documented that they the relaxivity response of GBCA can vary very significantly with complex size, making the methodology reported here very useful for the characterization of GBCA candidates.

Credit authorship contribution statement

Chutintorn Somnin : Investigation, Writing – original draft. Laurent Leclercq : Conceptualization, Supervision, Writing – review & editing. Joseph Chamieh : Conceptualization, Supervision, Writing – review & editing. Mael Le Menedeu : Investigation. Christelle Medina : Conceptualization, Supervision, Writing – review & editing. Olivier Rousseaux : Conceptualization, Supervision, Writing – review & editing.

Raphael Tripier : Supervision. Carlos Platas Iglesias : Investigation, Writing – original draft, Writing – review & editing. Hervé Cottet : Conceptualization, Supervision, Writing – review & editing.

Declaration of competing interest

The authors declare that they have no known competing financial interests or personal relationships that could have appeared to influence the work reported in this paper.

Acknowledgments

This work was supported by Guerbet under a cooperative research and development agreement with the University of Montpellier and the CNRS.

Appendix A. Supplementary data

Tables S1 presents the structure of the GBCA and PCTA ligands.

Fig. S1 displays TDA setup with UV and LEDIF detectors

Fig. S2. Emission spectra (excitation wavelength 275 nm) of Gd-PCTA, Gd-PCTA D1 and Gd-PCTA D2 at a concentration of 5.0 mM.

Fig. S3 to S10 present the taylorgrams obtained for Gd-DTPA-BMA, Gd-BOPTA, Gd-HP-DO3A, Gd-BT-DO3A, Gd-DOTA, Gd-PCTA, Gd-PCTA D1, Gd-PCTA D2 and Gd-PCTA D3, respectively.

Fig. S11 shows linear regression lines obtained for GBCA calibration curves in UV 200 nm and LEDIF (λ_{ex} 275 nm, $\lambda_{collection}$ 300-450 nm).

Tables S2-S12 show optimized geometries obtained with DFT.

References

Aime, S., Caravan, P., 2009. Biodistribution of gadolinium-based contrast agents, including gadolinium deposition. J. Magn. Reson. Imaging, 30, 1259-1267. https://doi.org/10.1002/jmri.21969.

Aris, R., 1956. On the dispersion of a solute in a fluid flowing through a tube. Proc. R. Soc. A. 235, 67–77. https://doi.org/10.1098/rspa.1956.0065.

Bader, R.F.W., Carroll, M.T., Cheeseman, J.R., Chang, C., 1987. Properties of atoms in molecules: atomic volumes. J. Am. Chem. Soc. 109, 7968-7979. https://doi.org/10.1021/ja00260a006.

Bello, M.S., Rezzonico, R., Righetti, P.G., 1994. Use of Taylor-Aris dispersion for measurement of a solute diffusion coefficient in thin capillaries. Science 266(5186), 773-776. https://doi.org/10.1126/science.266.5186.773.

Belongia, B.M., Baygents, J.C., 1997. Measurements on the diffusion coefficient of colloidal particles by Taylor-Aris dispersion. J. Colloid Interface Sci. 195, 19–31. https://doi.org/10.1006/jcis.1997.5131.

Bünzli, J.C.G., 2010. Lanthanide Luminescence for Biomedical Analyses and Imaging. Chem. Rev. 110, 2729-2755. https://doi.org/10.1021/cr900362e.

Caravan, P., 2006. Strategies for increasing the sensitivity of gadolinium based MRI contrast agents. Chem. Soc. Rev. 35, 512-523. https://doi.org/10.1039/B510982P.

Chai, J.D., Head-Gordon, M., 2008. Long-range corrected hybrid density functionals with damped atom–atom dispersion corrections. Phys. Chem. Chem. Phys 10, 6615–6620. https://doi.org/10.1039/b810189b.

Chamieh, J., Cottet, H., 2014. Chapter 9 - Size-based characterisation of nanomaterials by Taylor dispersion analysis. Colloid and Interface Science in Pharmaceutical Research and Development. H. Makino and K. Ohshima. Amsterdam, Elsevier, 173-192. https://doi.org/10.1016/b978-0-444-62614-1.00009-0.

Chamieh, J., Leclercq, L., Martin, M., Slaoui, S., Jensen, H., Ostergaard, J., Cottet, H., 2017. Limits in size of taylor dispersion analysis: representation of the different hydrodynamic regimes and application to the size-characterization of cubosomes. Anal. Chem. 89, 13487–13493. https://doi.org/10.1021/acs.analchem.7b03806.

Cottet, H., Biron, J. P., Martin, M., 2014. On the optimization of operating conditions for Taylor dispersion analysis of mixtures. Analyst 139(14), 3552-3562. https://doi.org/10.1039/c4an00192c.

Dolg, M., Stoll, H., Preuss, H., 1989. Energy-adjusted Ab Initio pseudopotentials for the rare earth elements. J. Chem. Phys 90, 1730−1734. https://doi.org/10.1063/1.456066.

d'Orlyé, F., Varenne, A., Gareil, P., 2008, Determination of nanoparticle diffusion coefficients by Taylor dispersion analysis using a capillary electrophoresis instrument, J. Chromatogr. A 1204 (2), 226-232. https://doi.org/10.1016/j.chroma.2008.08.008.

Dumas, S., Jacques, V., Sun, W.C., Troughton, J.S., Welch, J.T., Chasse, J.M., Schmitt-Willich, H., Caravan, P., 2010. High relaxivity magnetic resonance imaging contrast agents. Part 1. Impact of single donor atom substitution on relaxivity of serum albumin-bound

gadolinium complexes. Invest. Radiol. 45(10), 600-612. https://doi.org/10.1097/RLI.0b013e3181ee5a9e.

Esteban-Gómez, D., De Blas, A., Rodríguez-Blas, T., Helm, L., Platas-Iglesias, C., 2012. Hyperfine coupling constants on inner-sphere water molecules of GdIII -based MRI contrast agents. ChemPhysChem 13, 3640–3650. https://doi.org/10.1002/cphc.201200417.

Evans R., Deng Z., Rogerson, A.K., McLachlan, A.S., Richards, J.J., Nilsson, M., Morris G.A., 2013. Quantitative interpretation of diffusion-ordered NMR spectra: Can we rationalize small molecule diffusion coefficients?. Angew. Chem. Int. Ed. 52, 3199-3202. https://doi.org/10.1002/anie.201207403.

Frisch, M. J., Trucks, G. W., Schlegel, H. B., Scuseria, G. E., Robb, M. A., Cheeseman, J. R., Scalmani, G., Barone, V., Petersson, G. A., Nakatsuji, H., Li, X., Caricato, M., Marenich, A. V., Bloino, J., Janesko, B. G., Gomperts, R., Mennucci, B., Hratchian, H. P., Ortiz, J. V., Izmaylov, A. F., Sonnenberg, J. L., Williams-Young, D., Ding, F., Lipparini, F., Egidi, F., Goings, J., Peng, B., Petrone, A., Henderson, T., Ranasinghe, D., Zakrzewski, V. G., Gao, J., Rega, N., Zheng, G., Liang, W., Hada, M., Ehara, M., Toyota, K., Fukuda, R., Hasegawa, J., Ishida, M., Nakajima, T., Honda, Y., Kitao, O., Nakai, H., Vreven, T., Throssell, K., Montgomery, J. A., Jr., Peralta, J. E., Ogliaro, F., Bearpark, M. J., Heyd, J. J., Brothers, E. N., Kudin, K. N., Staroverov, V. N., Keith, T. A., Kobayashi, R., Normand, J., Raghavachari, K., Rendell, A. P., Burant, J. C., Iyengar, S. S., Tomasi, J., Cossi, M., Millam, J. M., Klene, M., Adamo, C., Cammi, R., Ochterski, J. W., Martin, R. L., Morokuma, K., Farkas, O., Foresman, J. B., Fox, D. J. Gaussian 16 Rev. C.01, Gaussian, Inc., Wallingford CT, 2016.

Hao, J., Bourrinet, P., Desché, P., 2019. Assessment of pharmacokinetic, pharmacodynamic profile, and tolerance of Gadopiclenol, a new high relaxivity GBCA, in healthy subjects and patients with brain lesions (phase I/IIa study). Invest. Radiol. 54(7), 396-402. https://doi.org/10.1097/RLI.0000000000000556.

He, X., Matsuki, X., Li, K., Sui, Y., Matsuno, K., Ren, M., Sutter, G., Hofmann, B.M., 2024. Pharmacokinetics, safety, and tolerability of the novel tetrameric gadolinium-based MRI contrast agent gadoquatrane in healthy Chinese and Japanese men: Two randomized dose-escalation studies including concentration–QTc modeling. Eur. J. Pharm. Sci. 196, 106749. https://doi.org/10.1016/j.ejps.2024.106749.

Jacquier, A., Bucknor, M., Do, L., Robert, P., Corot, C., Higgins, C.B., Saeed, M., 2008. P846, a new gadolinium based low diffusion magnetic resonance contrast agent, in characterizing occlusive infarcts, reperfused ischemic myocardium and reperfused infarcts in rats. Magn. Reson. Mater. Phys., Biol. Med. 21(3), 207-218. https://doi.org/10.1007/s10334-008-0112-8.

Kanda, T., Oba, H., Toyoda, K., Kitajima, K., Furui, S., 2016. Brain gadolinium deposition after administration of gadolinium-based contrast agents. Jpn. J. Radiol. 34(1), 3-9. https://doi.org/10.1007/s11604-015-0503-5.

Lauffer, R.B., 1987. Paramagnetic metal complexes as water proton relaxation agents for NMR imaging: theory and design. Chem. Rev. 87, 901-927. http://doi.org/10.1021/cr00081a003.

Le Fur, M., Rotile, N.J., Correcher, C., Clavijo Jordan, V., Ross, A.W., Catana, C., Caravan, P., 2020. Yttrium-86 is a positron emitting surrogate of gadolinium for noninvasive quantification of whole body distribution of gadolinium-based contrast Agents. Angew. Chem. Int. Ed. 59(4), 1474-1478. https://doi.org/10.1002/anie.201911858.

Le Fur, M., Moon, B.F., Zhou, I.Y., Zygmont, S., Boice, A., Rotile, N.J., Ay, I., Pantazopoulos, P., Feldman, A.S., Rosales, I.A., How, I.D.A.L., Izquierdo-Garcia, D., Hariri, L.P., Astashkin, A.V., Jackson, B.P., Caravan, P., 2023. Gadolinium-based contrast agent biodistribution and speciation in rats. Radiology 309(1), e230984. https://doi.org/10.1148/radiol.230984.

Le Mignon, M.M., Chambon, C., Warrington, S., Davies, R., Bonnemain, B., 1990. Gd-DOTA Pharmacokinetics and tolerability after intravenous injection into healthy volunteers. Invest. Radiol. 25, 933–937. https://doi.org/10.1097/00004424-199008000-00010.

Nucera, A., Platas-Iglesias, C., Carniato, F., Botta, M., 2023. Effect of hydration equilibria on the relaxometric properties of Gd(iii) complexes: new insights into old systems. Dalton Trans. 52, 17229-17241. https://doi.org/10.1039/D3DT03413E.

Pellegatti, L., Zhang, J., Drahos, B., Villette, S., Suzenet, F., Guillaumet, G., Petoud, S., Tóth, É., 2008. Pyridine-based lanthanidecomplexes: towards bimodal agents operating as near infrared luminescent and MRI reporters. Chem. Commun. 48, 6591-6593. https://doi.org/10.1039/B817343E.

Peterson, K.A., Figgen, D., Dolg, M., Stoll, H., 2007. Energy-consistent relativistic pseudopotentials and correlation consistent basis sets for the 4d elements Y–Pd. J. Chem. Phys. 126 (12), https://doi.org/10.1063/1.2647019.

Port Marc, Complexes métalliques de polyaminoacides bicycliques, leur procédé de préparation et leur application en imagerie médicale. French patent FR2794744A1. Issued December 15, 2000.

Port Marc, Compounds comprising short aminoalcohol chains and metal complexes for medical imaging. European patent EP1931673B1. Issued June 18, 2008.

Regueiro-Figueroa, M., Platas-Iglesias, C., 2015. Toward the prediction of water exchange rates in magnetic resonance imaging contrast agents: A density functional theory study. J. Phys. Chem. A 119, 6436–6445. https://doi.org/10.1021/acs.jpca.5b01728.

Spencer, A.J., Wilson, S.A., Batchelor, J., Reid, A., Pees, J., Harpur, E., 1997. Gadolinium Chloride Toxicity in the Rat. Toxicol. Pathol. 25, 245-255. https://doi.org/10.1177/019262339702500301.

Staks, T., Schuhmann-Giampieri, G., Frenzel, T., Weinmann, H. J., Lange, L., Platzek, J., 1994. Pharmacokinetics, dose proportionality, and tolerability of gadobutrol after single intravenous injection in healthy volunteers. Invest. Radiol. 29, 709–715. https://doi.org/10.1097/00004424-199407000-00008.

598 Taylor, G., 1953. Dispersion of soluble matter in solvent flowing slowly through a tube. Proc.
599 R. Soc. A 219(1137), 186-203. https://doi.org/10.1098/rspa.1953.0139.
600
601 Taylor, G.,1954. Conditions under which dispersion of a solute in a stream of solvent can be
602 used to measure molecular diffusion. Proc. R. Soc. A 225 (1163), 473-477.
603 https://doi.org/10.1098/rspa.1954.0216.
604
605 Tomasi, J., Mennucci, B., Cammi, R., 2005. Quantum mechanical continuum solvation
606 models. Chem. Rev. 105, 2999-3093. https://doi.org/10.1021/cr9904009.
607
608 Weigend, F., Ahlrichs, R., 2005. Balanced basis sets of split valence, triple zeta valence and
609 quadruple zeta valence quality for H to Rn: Design and assessment of accuracy. Phys. Chem.
610 Chem. Phys. 7, 3297–3305. https://doi.org/10.1039/b508541a.
611
612 Xu, J., Chen, Z., Yu, J.C., Tang, C., 2002. Simultaneous determination of inorganic anions,
613 carboxylic and aromatic carboxylic acids by capillary zone electrophoresis with direct UV
614 detection. J. Chromatogr. A 942, 289-294. https://doi.org/10.1016/S0021-9673(01)01402-9.
615
616 Xu, R.L., 2015. Light scattering: A review of particle characterization applications.
617 Particuology 18, 11-21. https://doi.org/10.1007/s10334-008-0112-8.